Journal of Biomedical Optics

BiomedicalOptics.SPIEDigitalLibrary.org

Comparative study of methods to calibrate the stiffness of a single-beam gradient-force optical tweezers over various laser trapping powers

Mohammad Sarshar
Winson T. Wong
Bahman Anvari

SPIE.

Journal of Biomedical Optics 19(11), 115001 (November 2014)

Comparative study of methods to calibrate the stiffness of a single-beam gradient-force optical tweezers over various laser trapping powers

Mohammad Sarshar, Winson T. Wong, and Bahman Anvari*
University of California, Department of Bioengineering, Riverside, California 92521, United States

Abstract. Optical tweezers have become an important instrument in force measurements associated with various physical, biological, and biophysical phenomena. Quantitative use of optical tweezers relies on accurate calibration of the stiffness of the optical trap. Using the same optical tweezers platform operating at 1064 nm and beads with two different diameters, we present a comparative study of viscous drag force, equipartition theorem, Boltzmann statistics, and power spectral density (PSD) as methods in calibrating the stiffness of a single beam gradient force optical trap at trapping laser powers in the range of 0.05 to 1.38 W at the focal plane. The equipartition theorem and Boltzmann statistic methods demonstrate a linear stiffness with trapping laser powers up to 355 mW, when used in conjunction with video position sensing means. The PSD of a trapped particle's Brownian motion or measurements of the particle displacement against known viscous drag forces can be reliably used for stiffness calibration of an optical trap over a greater range of trapping laser powers. Viscous drag stiffness calibration method produces results relevant to applications where trapped particle undergoes large displacements, and at a given position sensing resolution, can be used for stiffness calibration at higher trapping laser powers than the PSD method. [DOI: 10.1117/1.JBO.19.11.115001]

Keywords: Boltzmann statistics; equipartition theorem; power spectral density; viscous drag; charge-coupled diode camera; quadrant photodetector.

Paper 140218R received Apr. 5, 2014; revised manuscript received Sep. 16, 2014; accepted for publication Sep. 29, 2014; published online Nov. 6, 2014.

1 Introduction

Since its introduction by Ashkin,[1] optical tweezers have been used in a broad range of applications in biology,[2–16] physics,[17–23] and biophysics.[24–31] The pico-Newton force resolution offered by optical tweezers and its noninvasive nature render it as a useful instrument in cell manipulation[32–35] and force microscopy studies.[21] Use of optical tweezers in quantitative studies requires accurate calibration of the optical trap stiffness. Considerable efforts have been made in developing calibration techniques or improving their efficiency and accuracy.[36–53] In general, stiffness calibration methods for optical tweezers are divided into three categories. In the first category (also referred to as active stiffness calibration methods), optical trap stiffness is obtained by calibration of the laser-mediated optical force against a known externally applied force. An example of an applied external force is the Stokes' drag experienced by an optically trapped particle in response to relative movement between the trapped particle and the fluid in which the particle is trapped. Under this approach, either the trapping chamber is moved against a fixed optical trap or calibrated movements are applied to a steerable trapped particle within the trapping chamber.[5–10,53–57]

In the second (passive) stiffness calibration category, several calibration methods exist to estimate the stiffness of the optical tweezers by analyzing the thermal fluctuations of the trapped particle.[58] Position variance of a trapped particle is used to calculate the optical tweezers stiffness by modeling the behavior of the particle using the equipartition theorem. In another approach, the optical trap's potential is reconstructed using Boltzmann statistics.[58] Using this method, the stiffness is measured using the complete distribution of the trapped particle's positions within the optical trap.[59,60] Alternatively, using the power spectral density (PSD) method, a trapped particle's thermal noise is analyzed in the frequency domain to determine the optical trap's stiffness.[41]

The third (direct) category estimates the optical trap's stiffness by measuring the changes in momentum of scattered trapping light.[39,61,62] This approach usually requires a dual-beam trap and collection of the entire scattered light. The direct calibration method has recently been applied to single-beam traps[50,63] in conjugation with back focal plane interferometry, but is not yet commonly employed.

The absolute optical trap stiffness measured at a given trapping laser power depends on the calibration approach employed. Variations in reported trap stiffness have been attributed to uncertainties associated with the method used to calibrate the trap stiffness and can lead to discrepancies in reported forces associated with common biological phenomena.[64] Although comprehensive theoretical and experimental studies of each stiffness calibration approach are reported in the literature, a side-by-side study of such approaches in measuring an optical trap's stiffness over a range of trapping laser powers will help evaluate the efficacy of each calibration technique in practice and better understand the discrepancies among the stiffness values they report.

---

*Address all correspondence to: Bahman Anvari, E-mail: anvarib@ucr.edu

Detecting the displacements of a particle within the optical trap is a crucial part in all aforementioned calibration methods. Both low-bandwidth (<1 kHz) and high-bandwidth (usually in the range of 10 to 70 kHz) position sensing means are used to track the displacements of an optically trapped particle. We used a charge-coupled diode (CCD) camera as low-bandwidth and a quadrant photodetector (QPD) as high-bandwidth position detection means to assess the ability of low-bandwidth and high-bandwidth particle tracking schemes in calibrating optical trap stiffness over trapping laser powers in the range of ≈0.05 to 1.38 W. The QPD can be aligned either in a basic manner to track the image (or the shadow) of a trapped particle, much like in video particle tracking, or in an enhanced manner to track the trapped particle using the forward-scattered laser light off the particle. In the later configuration, the interference pattern resulting from unscattered trapping laser (or a second low-power tracking laser) and the forward-scattered laser lightsfrom the bead is projected onto the QPD at the back focal plane of the condenser lens.

The back focal plane interferometry configuration improves the spatial resolution beyond what the imaging configuration offers, but requires using a high numerical aperture (N.A.) condenser lens matching the N.A. of the trapping microscope objective in order to collect the entire scattered laser light. While the QPD can be used in imaging mode for particle tracking in virtually any optical trapping setup, the use of forward-scattered light is limited because of its necessary design considerations and optics. As an example, when optical tweezers are combined with other modes of biophysical experimental techniques, such as patch clamp,[65] a high N.A. condenser can no longer be used to collect the scattered laser light for particle tracking.

In this study, we utilized an optical tweezers setup with design considerations applicable to most common biophysical investigations and used different calibration methods to compare the transverse stiffness of the trap over various trapping laser powers. We first obtained the optical trap stiffness by applying known viscous drag forces against an optically trapped polystyrene bead at various laser output powers (i.e., active stiffness calibration method). To compare with the passive stiffness calibration methods, we performed a series of calibration experiments based on the PSD, equipartition theorem, and Boltzmann statistics methods over the same range of trapping laser powers.

Stiffness of an optical trap changes with the size of the optically trapped particle. The maximum optical trapping forces experienced by beads (micro- or nano-sized spheres) have a nonlinear correlation with the bead radius (r). For a trapping laser wavelength of $\lambda = 1064$ nm, maximum optical forces experienced by small volume ($r < 100$ nm) trapped beads have been shown to increase to the third power of the radius (r^3) in the Rayleigh regime,[36,66] with the exponent decreasing beyond the 100 nm range.[67] For beads with large volumes ($r > 10\ \mu$m) the maximum optical force experienced by the particle decreases with an inverse relation to its radius.[68]

Significant attempts have been made to model the trapping optical forces experienced by a particle in different volume scales. Earlier models[69] suggested that the size dependency of the maximum trapping forces experienced by beads can be described using the electromagnetic theory in the small-volume scale and ray optics in the large-volume scale. The mid-volume scale particles that are most commonly used in biophysical studies were first successfully included in a multiscale electromagnetic model by Rohrbach,[70] who studied the optical trap stiffness as a function of the bead radius in the range of 0.11 to 0.5 μm. Neto and Nussenzveig used the Mie theory to model the axial[71] and transverse[72] optical trapping forces on beads, which can also be expanded to predict the optical forces on particles in the ray optics regime. Accuracy of such multiscale models is improved by further optical characterizations of the tweezers setup, such as accounting for spherical aberrations[73] and astigmatism.[74]

In addition to the radius-dependent differences in how particles in different volume-scales interact with the highly focused laser in optical traps, other particle characteristics, such as the refractive index[68] and polarizability,[75] affect the optical trap stiffness as well. Moreover, it has been recently shown that the dynamic behavior of optically trapped microparticles in viscous media transitions from an overdamped regime for larger particles ($r > 1\ \mu$m) to an underdamped regime for smaller particles ($r < 250$ nm).[76]

Herein, we have used particles of two different sizes within the Mie regime and compared the results of different calibration methods on particle size dependence of the optical trap stiffness. Under the high-bandwidth position sensing scheme, we calibrated the optical trap stiffness using the PSD and viscous drag force methods. We used the equipartition theorem and Boltzmann statistic calibration methods to calibrate the optical trap stiffness under the low-bandwidth position detection scheme. We demonstrate that employing different calibration methods and position sensing means report different stiffness values for an optical trap, and discuss practical advantages and disadvantages of each approach.

2 Methods

2.1 *Experiment Setup*

2.1.1 *Optical trap formation*

Schematic of the experimental setup is shown in Fig. 1. The optical trap was formed on an inverted microscope (Ti-Eclipse, Nikon Inc., Melville, New York) using a 100× oil immersion objective lens with 1.49 N.A. and 120 μm working distance (Apo TIRF, Nikon). A solid-state Nd∶YVO$_4$ laser (Prisma 1064-V, Coherent, Santa Clara, CA) generating a laser beam with a 1064 nm wavelength in TEM$_{00}$ mode was used for optical trapping. The laser beam was expanded by a set of plano-convex lenses to slightly overfill the back aperture of the microscope objective. The output power of the trapping beam was measured at the back aperture of the objective lens by a power meter (PD300, Ophir Optronics, North Andover, MA). We used beads with two different diameters for trapping. The smaller beads were sulfate-modified fluorescent polystyrene beads 4.2 ± 0.21 (mean ± standard deviation) μm in diameter (F-8858, Molecular probes, Eugene, OR). These beads had an excitation spectrum between 480 and 590 nm with peak fluorescence emission at 605 nm when photo-excited at 580 nm. We refer to these particles as red beads. In addition to the 4-μm-diameter red beads, we used larger polystyrene beads, approximately twice in diameter ($8 \pm 0.7\ \mu$m; 2106E, Phosphorex, Hopkinton, MA) while maintaining a comparable position tracking signal-to-noise ratio (SNR) between the experiments. These beads had an excitation spectrum between 400 and 490 nm with peak fluorescence emission at 500 nm when photo-excited at 460 nm. We refer to these particles as green beads. Both particles were chosen within the same volume-scale to limit the uncertainties related to the volume-dependent differences in how particles in different volume-scales interact

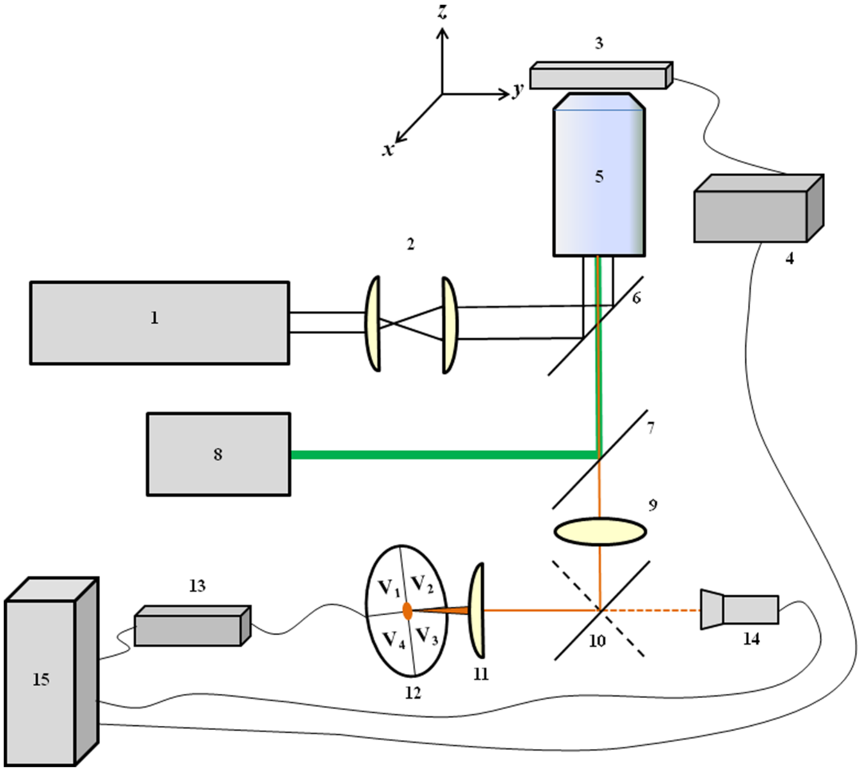

Fig. 1 Schematic of the experimental setup. (1) Nd:YVO$_4$ laser. (2) Beam expander. (3) piezoelectric translation (PZT) stage. (4) PZT controller. (5) 100× microscope objective. (6) Dichroic mirror. (7) TRITC/FITC filter set. (8) Arc lamp. (9) Condenser. (10) Steering mirror. (11) Focusing optics. (12) Quadrant photodetector. (13) Analog to digital converter. (14) CCD camera. (15) Computer.

with the highly focused laser in optical traps. Beads were suspended in deionized (DI) water during optical trapping experiments.

The trapping laser beam (1064 nm) can give rise to two-photon absorption phenomena in red fluorescent beads over all trapping laser powers. To investigate the effects of two-photon absorption on the measured stiffness, we repeated the trap stiffness calibrations using a control bead that had material properties and drag coefficient similar to those of the red fluorescent beads, but without significant two-photon absorption over the trapping laser powers. Specifically, we used 4.18 ± 0.4-μm-diameter dragon green fluorescent beads (Bangs Laboratories Inc., Fishers, IN) with peak absorption and emission at 480 and 520 nm, respectively. We repeated the trap stiffness calibrations using the viscous drag force method over the low (50 and 136 mW), medium (674 mW), and high (1.38 W) laser powers (delivered at the specimen plane) in samples containing both 4 μm beads, with results presented in Sec. 3.2.1. We used a dichroic beam splitter with >90% transmittance between 470 and 650 nm, and >98% reflectance at 1064 nm (680dcspxr-laser, Chroma Technology Corp, Bellow Falls, VT) to stir the laser beam toward the objective. The optical setup allowed for simultaneous trapping and fluorescent imaging of the trapped beads.

The transmissions of the microscope objective at 1050 and 1100 nm are reported by the manufacturer as 60% and 57%, respectively. We assumed a 60% transmission for the objective lens at 1064 nm, which is in agreement with other reports[77–79] that measured the transmittance of high N.A. microscope objectives of the same brand and similar optical properties at 1064 nm using the dual objective method.[79–81] We increased the laser output power in eight steps from 85 mW to a maximum power of 2.294 W, measured at the back pupil of the objective. The calculated trapping laser powers delivered to the specimen plane ranged between 50 mW and 1.38 W.

We measured the temperature of the DI water using a thermistor connected to a Vernier LabQuest device (Vernier Software & Technology, Beaverton, OR). The mean ± standard deviation value of water temperature was 24.98 ± 0.23°C (water dynamic viscosity $\eta = 0.8925 \cdot 10^{-3}$ Pa · s at $T = 24.98$°C). The laser-induced temperature increase, which occurs within the laser focus, has a significant effect on the measured trap stiffness through its effect on the viscosity of the medium and the thermal motion of the trapped particle.[78,82] This effect becomes more pronounced at higher trapping laser powers and higher trapping depths when using an oil immersion microscope objective.[83] We accounted for these effects by assuming a temperature increase of 8 K/W at 1064 nm in DI water as our optical trapping medium.[78] Therefore, the expected range of the DI water temperature in our experiments during the applied range of trapping powers was ≈24.98 to 35.99°C. Furthermore, all experiments were conducted within 30 s of the initial trapping of the bead to avoid or minimize excessive temperature buildup at laser focus.

2.1.2 *Fluorescence and bright field imaging and position detection*

Both white light and fluorescence modes can be used for particle tracking using the QPD in the imaging configuration. Under white light, the contrast between the shadow of the optically trapped particle and the bright background is used for particle tracking. In fluorescence, the emission from a fluorescent probe against the dark background is used to track the optically trapped fluorescent particle. For bright field imaging of the particles, a 100 W tungsten lamp (TI-DH Diascopic Illumination Pillar, Nikon) was used to illuminate the samples. For fluorescence imaging of the particles, an arc lamp (LUDL Electronic products, Hawthorne, NY) was used to optically excite the fluorescent beads.

We used a TRITC-B-NTE filter set (Semrock, Rochester, NY) to optically excite the red fluorescent beads in the 530 to 550 nm band and collect the fluorescence emission in the 570 to 620 nm range. A FITC-3540B-NTE filter set (Semrock), which allows the transmission of an excitation band in the range of 446 to 500 nm and an emission band of 513 to 725 nm, was used during the optical excitation of the green fluorescent beads and collection of fluorescence emission. For comparative purposes, we employed two commonly used position sensing methods: first, a nonvideo position detection using a QPD (QP50-6SD, Pacific Silicon Sensor, Westlake Village, CA) and second, video particle tracking using a CCD camera (C9100-13, Hamamatsu Corp., Bridgewater, NJ).

Using the QPD allowed for high-bandwidth position recordings with sampling frequencies in the kilohertz range. The QPD was aligned such that the image positions along the primary x, y, and z axes of the lab were, respectively, proportional to differential voltages $V_x = (V_1 + V_4) - (V_2 + V_3)$, $V_y = (V_3 + V_4) - (V_1 + V_2)$, and the sum voltage $V_S = V_1 + V_2 + V_3 + V_4$ (where V_{1-4} are diode voltages). Differential voltages were digitized by an analog-to-digital converter (BNC-2110 and NI PCI-6133, National Instrument, Austin, TX) and stored in a computer using LabVIEW software (version 8.2, National Instruments) for further analysis. Additionally, bead positions were determined using a CCD camera. For this purpose, images of the fluorescent bead were acquired at 179 frames per second (fps) by HCImage software (version 2.0, Hamamatsu) and analyzed in MATLAB® (The MathWorks, Natick, MA) for particle tracking.

2.2 *Displacement Calibrations*

2.2.1 *QPD-based position sensing*

To accurately control the position of the optical trapping chamber and apply viscous drag forces of known magnitude on trapped particles, we used a piezoelectric translation (PZT) stage (P-527.C3, Physik Instrumente, Waldbronn, Germany) with a transverse resolution of <10 nm. Output voltage of the QPD was calibrated against displacement using the PZT as follows. The position of a trapped bead in the field of view was initially taken as the reference point to center the QPD. Subsequently, in the absence of the optical trap, a bead was attached to the cover slip and brought to the exact transverse position of the trapped bead using the PZT. The fluorescent image of the bead (or the shadow of the bead when white light was used for particle tracking) was centered on the QPD by moving the QPD using a three-dimensional translational stage.

Next, the bead was displaced multiple times in steps of known increments (0.01 to 1 μm) using the PZT while QPD's differential voltages were recorded. Recording of larger bead displacements (up to 1 μm) in x and y directions showed that the QPD response within this range was linear. Finally, a linear fit to the displacement-voltage data points provided a voltage-displacement calibration equation for the QPD. The differential voltages V_x and V_y were normalized by V_S to create normalized output-displacement calibration graphs in x and y directions. The slope of the linear fit to the voltage-displacement graphs was used to convert QPD outputs to bead displacement during stiffness calibrations.

The two-photon fluorescence of the red fluorescent beads increases with the trapping laser power. Moreover, it has been shown that the axial position of the laser beam changes with the laser power as a result of laser-induced thermal expansions in the microscope objective,[84] affecting the position calibration. For the case of particles with strong two-photon absorption/emission, the laser power related differences in the displacement calibration coefficients become more prominent under white light and at higher trapping laser powers as the image of the trapped particle tends to fade away with the increased fluorescence. Therefore, it is important to obtain a separate displacement-calibration curve for the QPD at each trapping laser power.

The choice between using white light and fluorescence for particle tracking is based on the specific conditions of the intended experiments. Moreover, the quality and maximum resolution of the particle tracking scheme is related to the positional SNR, which in turn depends on the characteristics of optically trapped probe and the detector's spectral sensitivity. For example, our group has used 800 and 1064 nm optical tweezer setups to conduct biophysical studies of cell membranes by extracting membrane tethers from cells using optically trapped particles.[28–30] The shadow cast by the membrane tether introduces large errors in position sensing under white light. To overcome this obstacle while maintaining the SNR, we use fluorescent probes with an emission band in a region where our QPD has a high spectral sensitivity (~600 nm). In fact, the position tracking SNR for the red fluorescent beads increases by ~8% in our system when switching from the white light mode to the fluorescence. However, the emission band of the dragon green fluorescent particles used in Sec. 3.2.1 coincides with an area of poor spectral sensitivity of our QPD, resulting in low SNR for tracking these particles in fluorescence mode. Therefore, the QPD position detection in these experiments was conducted in bright field.

2.2.2 *Video-based position sensing*

Images acquired by the CCD camera were spatially calibrated by imaging a microruler with 10 μm spacing. Although the pixel resolution of our CCD imaging system is diffraction limited, there are a number of algorithms for spherical objects[85,86] that can estimate the centroid of the particle to subpixel accuracy, thereby increasing the spatial resolutions of video particle tracking to nanometer range.

We used the radial symmetry method developed by Parthasarathy[86] to track the position of the optically trapped particles to subpixel resolution. The results of the video-based position sensing are ultimately dependent on the accuracy and pixel noise levels associated with the particle tracking algorithm used. To demonstrate this matter, we adopted the interactive data language algorithm for the centroid method developed by Crocker and Grier[87] for MATLAB® to track the position of the beads in the same sets of CCD images used in the radial symmetry method. An example of the stiffness values calculated using the two particle tracking algorithms is provided in the Results section. Since the image exiting the microscope objective was slightly diverging, the pixel calibration was sensitive to the position of microscope objective. Therefore, we performed a calibration against an in-focus microruler by averaging the pixel size while the height of the stage (and, therefore, that of the objective) was changed in a range of 30 μm (covering the actual positions of microscope objective during stiffness calibrations).

2.3 *Stiffness Calibrations*

Both the trap stiffness and the magnitude of the viscous drag force applied by the trapping medium on an optically trapped particle depend on the distance of the trapped object from the bottom of the trapping chamber.[47] The viscous drag force experienced by a particle in a moving viscous medium is given as[36]

$$F_{\text{drag}} = \beta \cdot \nu = \frac{6\pi\eta\nu r}{1 - \frac{9}{16}\left(\frac{r}{h}\right) + \frac{1}{8}\left(\frac{r}{h}\right)^3 - \frac{45}{256}\left(\frac{r}{h}\right)^4 - \frac{1}{16}\left(\frac{r}{h}\right)^5}, \tag{1}$$

where β (kg/s) is the drag coefficient, r (m) is the radius of the bead, ν (m/s) is the fluid velocity, and h (m) is the height of the bead from the bottom of the dish.

The displacement of the laser focus in the trapping media resulting from axial displacements of the microscope objective (along the propagation axis of the trapping beam) was calibrated using the PZT stage. Prior to each experiment, the trapped bead was brought in contact with the cover slip by moving the tapping chamber in the axial (z) direction and then raised by 16 and 30 μm above the cover slip using the PZT for experiments with the 4 and 8 μm beads, respectively. As V_S remained unchanged in the span of data collection for each experiment (30 s), the position of the trapped bead along the laser propagation axis was assumed to remain constant. Minor axial displacement of the bead within the Rayleigh depth of focus of our system was neglected since at the height of 30 μm above the cover slip, it could only contribute to 0.03% change in the drag coefficient, β.

2.3.1 *Active stiffness calibration based on viscous drag force method*

Forces applied on a microsphere in the proximity of the trapping chamber's bottom can be calculated using Eq. (1). Holding the trapped bead at a constant height above the cover slip, we moved the PZT stage at controlled velocities to induce known viscous forces on the optically trapped microsphere based on Eq. (1). Displacement of the bead from the center of the trap was recorded as a differential voltage by the QPD. These voltages were converted to displacements using the voltage-displacement equations. The resulting data for displacement-force graph were linearly fitted for small displacements from the center of the trap (<1 μm) using $f = -k \cdot x$, where the stiffness of the trap (k) is extracted from the slope of the fit.

2.3.2 *Passive stiffness calibration method based on power spectral density method*

The Brownian motion of a particle in an optical trap can be described by the Langevin equation. For particles in fluids with low Reynolds numbers, the power spectrum of the Brownian motion is a Lorentzian function.

$$S(f) = \frac{K_B T}{\pi^2 \beta (f^2 + f_0^2)}, \tag{2}$$

where f (Hz) is frequency and f_0 is the roll-off frequency of the Lorentzian curve. Parameter f_0 can be extracted by plotting the PSD of the Brownian motion of the bead, which is then used to calculate the stiffness (k) of the optical trap (in either x or y direction) knowing the hydrodynamic drag coefficient β as

$$k = 2\pi\beta f_0. \tag{3}$$

The position sensing method used in this approach should be able to acquire data at frequencies that are considerably higher than the optical trap's roll-off frequency. Position samplings at 10 to 50 kHz are commonly reported in the literature. Although high-speed cameras along with algorithms that account for the aliasing and blur artifacts intrinsic to camera position sensing have been implemented in studying the PSD of an optical trap,[45,88,89] the use of such apparatus in the absence of multiple or drifting optical traps is not common. Instead, high-bandwidth nonvideo position sensing is commonly employed for stiffness calibration using PSD at a higher accuracy and a lower equipment cost. Our video position sensing system cannot be used to study the full spectrum of the PSD because its acquisition frequency (179 Hz) is well below the roll-off frequency of our optical trap. For stiffness calibration using the PSD method, we used the QPD position data recorded at 50 kHz. A MATLAB® application developed by Tolic-Nørrelykke et al.[42] was used to accurately extract the roll-off frequency, with results discussed in Sec. 3.

2.3.3 *Passive stiffness calibration based on equipartition theorem method*

Equipartition theorem assumes $0.5\,K_B T$ of thermal energy for each degree of freedom, where K_B is the Boltzmann constant ($\approx 1.38 \times 10^{-23}\ \mathrm{J\,K^{-1}}$) and T (K) is the absolute temperature. On the other hand, energy associated with thermal fluctuations of a particle in an optical trap with stiffness k_x in x direction equals $0.5\,k_x \langle x^2 \rangle^{-1}$, where $\langle x^2 \rangle$ is the position variance of the trapped particle in the x direction. By calculating the position variance of the trapped bead, we can measure the trap stiffness along the x axis (k_x) as

$$k_x = K_B T \langle x^2 \rangle^{-1}. \tag{4}$$

Similarly, we can measure the trap stiffness in the y direction (k_y) using the particle position variance along the y axis. This method of determining the trap stiffness requires a calibrated position sensing device, but does not require calculating the drag coefficient of the trapped bead or knowing the viscosity of the trapping medium. We recorded the position of the bead in the trap using the CCD camera, with stiffness calibration results presented in Sec. 3.

2.3.4 *Passive stiffness calibration based on Boltzmann statistics method*

In the classical Boltzmann statistics approach, the trapped particle's position histogram is assumed to have a normal distribution resulting from a Gaussian trapping laser beam. In thermal equilibrium, Boltzmann statistics describes the probability density $p(x)$ of the particle position as a function of the optical trap's potential $E(x)$.[58]

$$p(x)dx = Ce^{-\frac{E(x)}{K_B T}}, \tag{5}$$

where C is a normalization factor. Normalized histogram of the particle's positions in the optical trap is used to calculate the potential energy function:

$$E(x) = -K_B T \ln p(x) + K_B T \ln C. \tag{6}$$

The contribution of dx is incorporated in C, the normalization factor, and represented in the second term in Eq. (6). This term is an energy offset and is neglected by assuming zero potential at the center of the optical trap. To determine the potential energy, the logarithm of the function fitted to the calculated distribution of particle positions is taken and multiplied by $-K_B T$. The resulting distribution is fitted by a quadratic equation $E(x) = (k_x/2)x^2 + c$, where k_x is the trap stiffness along the x axis and c is an energy offset assumed to be zero. The trap stiffness along y axis is measured in the same way as that along the x axis.

By assuming a normal distribution for the trapped particle's position histogram and fitting a parabola to the logarithm of the normal distribution, the results calculated by the Boltzmann statistics method become identical to those by the equipartition theorem. In theory, this approach can enhance the reconstruction of the optical trap potential by relying on the wings of the position histogram. However, this advantage is absent in practice because of the relatively small counts in the wings of the histogram (especially at higher trapping laser powers), rendering them as sources of additional uncertainty. Moreover, the spatial mode of the trapping laser may be perturbed by other modes at high laser output powers, resulting in a non-Gaussian energy distribution across the diameter of the optical trap.

Therefore, we modified the Boltzmann statistics approach by fitting the trapped particle's position histogram using a kernel function with a smoothing bandwidth of ~1 nm instead of a Gaussian function. We then numerically took the logarithm of the function fitted to the calculated distribution of particle positions and multiplied it by $-K_B T$. Instead of fitting the resulting potential distribution function with a parabola, we numerically took the position derivative of the energy function. The trap stiffness was measured from the slope of a linear fit to the resulting displacement-force distribution over a region equivalent to one standard deviation away from the center of the trap where a linear distribution was generally observed. We present the stiffness calibration results of the modified Boltzmann statistics approach in Sec. 3. Calibrating an optical trap using the Boltzmann method does not require knowing the trapped particle's shape, drag coefficient, or medium's viscosity. We applied the Boltzmann statistics calibration method to the same position data sets recorded for the equipartition theorem calibration method using the CCD camera.

3 Results

3.1 *Displacement Calibrations*

3.1.1 *QPD-based position sensing*

Bead movements with steps as small as 10 nm were resolvable by the QPD. Voltage-displacement curves showed a linear QPD response for bead displacements <1 μm from the center of the optical trap.

Normalizing the differential voltage of the x and y channels by V_S did not improve the linear fits to the voltage-displacement data, mainly due to the absence of large axial displacements. While normalization decreases the susceptibility of linear fits to ambient optical noise, it also makes the slope of the fit dependent on background brightness. Therefore, in controlled experimental environments like ours with negligible changes in the background signal and the trapped particle's axial position, using the single differential voltages V_x and V_y (as opposed to normalized QPD outputs) is preferred.

The QPD displacement calibration coefficients for the 4 and 8 μm green fluorescent beads, respectively, changed by 8% and 4% under the fluorescence mode over the range of trapping laser powers in this study. These coefficient changes increase to 19% and 6% for the 4 and 8 μm green fluorescent beads under the white light, respectively. For the case of the 4 μm red fluorescent beads, the QPD displacement calibration coefficients vary over the trapping laser powers by 22% in fluorescence mode and 37% in the bright field mode. While we did not use the normalized QPD outputs, it should be noted that in all cases, normalization of the differential QPD voltages by V_S decreased the dependency of the displacement calibration coefficient on the trapping laser power in an arbitrary manner but did not eliminate it.

3.1.2 *Video-based position sensing*

Pixel calibration resulted in 158 nm/pixel in both x and y directions. The bead's centroid position was estimated with subpixel accuracy using the particle tracking algorithms. Data recorded from a stationary 4 μm bead attached to a cover slip showed a displacement noise of ~0.03 pixels for the radial symmetry and 0.06 pixels for the centroid methods corresponding to 4.7 and 9.5 nm, respectively. This value was measured as 0.042 pixels for the 8 μm beads using the radial symmetry method, corresponding to 6.6 nm.

3.2 *Stiffness Calibrations*

Each of the calibration methods discussed in this report calibrates the optical trap's transverse stiffness through the same procedure for both x and y directions. The results in the y direction followed the same trends as the results in the x direction in all calibration methods. Because the goal of this study is to provide a side-by-side comparison between the stiffness calibration methods, for simplicity, we present the trap stiffness measured by each calibration approach in only one of the principle directions, x.

3.2.1 *Active stiffness calibration method based on viscous drag force*

In Fig. 2, we present the optical trap stiffness for the 4 and 8 μm beads as a function of laser power delivered to the specimen plane using the active stiffness calibration method based on application of viscous drag force. Each point in the graph is extracted from the slope of a linear fit to the displacement-force graph obtained at the corresponding laser power (Fig. 2, inset). The stiffness values of our optical trap for the 4 μm beads ranged from $63.7 \pm 2.9\ \mathrm{pN} \cdot \mu\mathrm{m}^{-1}$ at 50 mW to $771.1 \pm 69.9\ \mathrm{pN} \cdot \mu\mathrm{m}^{-1}$ at 1.38 W, while the stiffness values for the 8 μm beads ranged from $51.6 \pm 8.5\ \mathrm{pN} \cdot \mu\mathrm{m}^{-1}$ at 50 mW to $733.8 \pm 78.8\ \mathrm{pN} \cdot \mu\mathrm{m}^{-1}$ at 1.38 W. As expected, a linear increase in optical trap stiffness was observed for both beads as the laser power increased. If not accounted for, the laser-induced temperature increase results in an overestimation of optical trap stiffness, which progressively increases with trapping power.

The average standard deviation from the mean stiffness values measured for the 4 μm bead is 7.6%. The average standard deviation increases to 12.7% for the 8 μm bead. These values are comparable with the uncertainties in the particle sizes

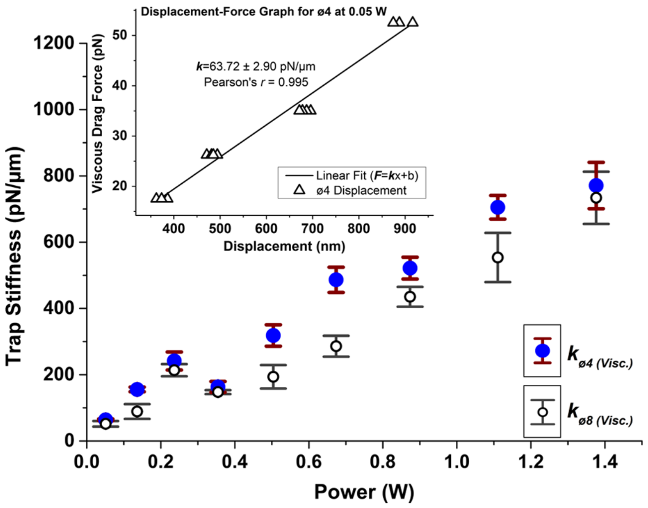

Fig. 2 Trap stiffness as a function of laser power at the specimen plane, using the active calibration method based on application of viscous drag force. The $k_{Ø4\,(\mathrm{Visc.})}$ data points (represented as larger filled circles) and $k_{Ø8\,(\mathrm{Visc.})}$ data points (represented as smaller unfilled circles) correspond to the estimated stiffness values of 4 μm red and 8 μm green fluorescent beads, respectively. The inset shows a typical displacement-force graph for the 4 μm red beads at 0.05 W. The Ø4 data points (shown as unfilled triangles) represent bead displacements from the center of the trap resulting from calculated viscous drag forces. The error bars to the mean estimated stiffness values using the red and green fluorescent beads are represented by thick vertical lines with short horizontal caps and thin vertical lines with long horizontal caps, respectively.

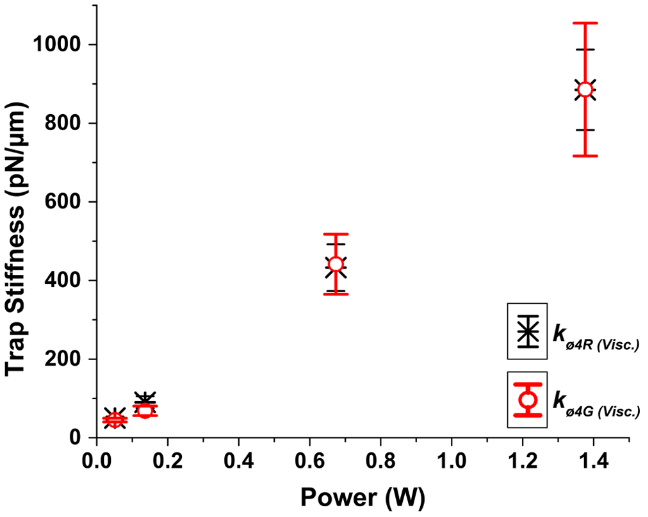

Fig. 3 Trap stiffness as a function of laser power at the specimen plane, using the active calibration method based on application of viscous drag force. The $k_{Ø4R\,(\mathrm{Visc.})}$ data points (represented as asterisks) and $k_{Ø4G\,(\mathrm{Visc.})}$ data points (represented as circles) correspond to the estimated stiffness values of 4 μm red and 4 μm dragon green beads under white light, respectively. The error bars to the mean estimated stiffness values using the red and dragon green fluorescent beads are represented by thin vertical lines with short horizontal caps and thick vertical lines with long horizontal caps, respectively.

(5 and 8.75% for the 4 and 8 μm beads, respectively). The large Pearson's r value (0.995) of the linear fit to the displacement-force graphs show that the optical trap behaves as a linear spring for bead displacements <1 μm (Fig. 2, inset). Thus, optical trap stiffness calibration based on viscous drag force does not suffer the theoretical or numerical approximations in modeling the optical trap behavior associated with the other calibration approaches used in this study.

The viscous drag force calibration method reports stiffness values for the 8 μm beads that are, on average, 23% less than those of the 4 μm beads across the laser powers used in this study. The stiffness values are directly extracted from the displacement-force graphs involving controlled external forces and report the smallest standard deviations compared with the other calibration methods used in this study. Therefore, we regard the trap stiffness calculated using the viscous drag force method as the most accurate and reproducible optical trap stiffness values in our experiments.

We repeated the trap stiffness calibrations in samples consisting of the 4.2 ± 0.21 μm red fluorescent beads and the 4.18 ± 0.4 μm dragon green fluorescent beads to investigate the effect of two-photon absorption on the measured stiffness. Figure 3 shows the results of the trap stiffness calibrations using the viscous drag force method over the low, mid, and high laser powers for both beads. The $k_{Ø4R\,(\mathrm{Visc.})}$ and $k_{Ø4G\,(\mathrm{Visc.})}$ data points correspond to the estimated stiffness values of 4 μm red and 4 μm green beads under white light, respectively. The difference between the mean stiffness values calculated using the two beads at each trapping laser power was smaller than the sum of standard deviations to the means and ranged from 10.6% at 50 mW to <0.01% at 1.38 W. Thus, the effects of two-photon absorption on the optical forces and the measured stiffness using particles in this volume-scale are negligible.

3.2.2 *Passive static calibration based on power spectral density method*

To find the characteristic roll-off frequency (f_0) of the optical trap, we recorded the position of 10 sequentially trapped beads of either diameter at various laser powers at a sampling rate of 50 kHz. We analyzed the PSD of bead displacements using an application developed by Tolic-Nørrelykke et al.[42] Data sets recorded for 10 s, and cropped at 5 and 2 s yielded the same roll-off frequencies. The roll-off frequencies for the experiments using the 4 μm beads were measured in the range of 255.6 ± 66 Hz at a trapping laser power of 50 mW to 1422 ± 256 Hz at 504 mW. The roll-off frequencies using the 8 μm beads were measured to range from 195 ± 30.3 Hz at 50 mW to 830.1 ± 64.9 Hz at 504 mW. Taking the effects of laser-induced temperature increase into consideration, these roll-off frequencies correspond to stiffness values in the range of $60.2 \pm 16\ \mathrm{pN} \cdot \mu\mathrm{m}^{-1}$ at 50 mW to $276.6 \pm 39.1\ \mathrm{pN} \cdot \mu\mathrm{m}^{-1}$ at 504 mW for the 4 μm beads, and $40.3 \pm 7.9\ \mathrm{pN} \cdot \mu\mathrm{m}^{-1}$ at 50 mW to $161.5 \pm 11\ \mathrm{pN} \cdot \mu\mathrm{m}^{-1}$ at 504 mW for the 8 μm beads.

Figure 4 shows the optical trap stiffness calculated for the 4 and 8 μm particles using the PSD method. The correlation between the trap stiffness and laser powers is linear up to the trapping laser power of 504 mW. However, at higher trapping powers, the uncertainty in the estimated stiffness values by the PSD calibration method increases, with reduced sensitivity of the stiffness estimates to power increments and deviation from a linear trend. This observation is in agreement with the previous reports that employed this stiffness calibration method.[78] The maximum laser trapping power range at which the PSD calibration method could be used to estimate reproducible stiffness calibration results was higher than the other two passive calibration

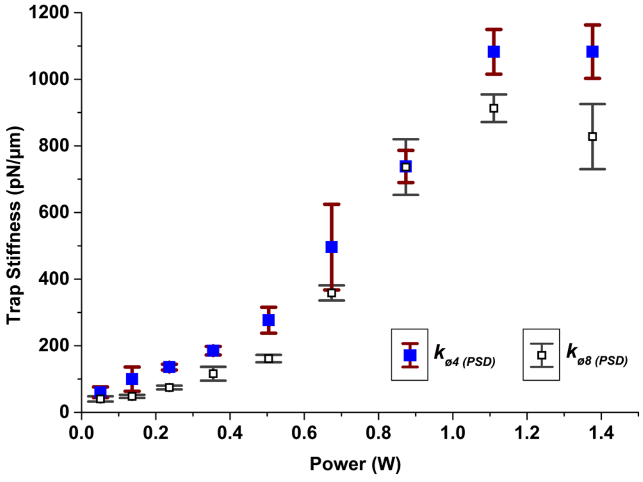

Fig. 4 Trap stiffness as a function of laser power at the specimen plane, using the passive stiffness calibration method based on the power spectral density. The $k_{Ø4\,(\mathrm{PSD})}$ data points (represented as larger filled squares) and $k_{Ø8\,(\mathrm{PSD})}$ data points (represented as smaller unfilled squares) correspond to the estimated stiffness values of 4 μm red and 8 μm green beads, respectively. The standard deviation from the mean measured stiffness values using the red and green fluorescent beads at each trapping laser power are represented by thick vertical lines with short horizontal caps and thin vertical lines with long horizontal caps, respectively.

methods as shown in the next section, but lower than the active stiffness calibration method. Within this range, the PSD method reports stiffness values for the 8 μm bead that are, on average, 42% smaller than those reported for the 4 μm bead. The average standard deviations from the mean stiffness values calculated for the 4 and 8 μm beads using the PSD method were 18 and 12%, respectively.

3.2.3 *Passive stiffness calibration based on equipartition theorem*

Using the variance of bead displacements as observed by the camera, the optical trap stiffness values for the 4 μm beads were estimated in the range of $36.8 \pm 7.5\ \mathrm{pN} \cdot \mu\mathrm{m}^{-1}$ at 50 mW of trapping laser power in the focal plane to $192 \pm 59.6\ \mathrm{pN} \cdot \mu\mathrm{m}^{-1}$ at 355 mW. The stiffness values for the 8 μm beads were estimated in the range of $38.9 \pm 18\ \mathrm{pN} \cdot \mu\mathrm{m}^{-1}$ at 50 mW to $196.5 \pm 64.6\ \mathrm{pN} \cdot \mu\mathrm{m}^{-1}$ at 355 mW [Fig. 5(a)]. The trap stiffness calculated by the equipartition theorem is in good agreement with the stiffness measured using the other methods at lower trapping laser powers. While video particle tracking at 179 fps was able to measure the optical trap stiffness using the equipartition theorem at trapping laser powers of up to 355 mW and observe a linear increase in the measured trap stiffness versus laser power, the method lost sensitivity to the increments in the trapping laser power beyond 355 mW, and no consistent results were reported at higher laser powers [Fig. 5(b)].

Optical trap stiffness calibration methods based on measuring the Brownian displacements of an optically trapped particle are highly dependent on accurate position sensing and easily disturbed by the presence of displacement noise. The accuracy of the stiffness values reported by this statistical calibration approach can be improved at higher trapping laser powers by enhancing the position detection's spatial and temporal resolution. Estimated optical trap stiffness by the equipartition theorem method has a direct correlation with the absolute temperature of the trapping medium [Eq. (4)]. The estimated 2.83 K temperature increase at 355 mW attributes to <1% underestimation of stiffness if the laser-induced temperature increase is neglected. The equipartition theorem calibration method reports stiffness values for the 8 μm bead that are, on average, 6% smaller than those reported for the 4 μm bead in its effective range of 50 to 355 mW. The average standard deviations from the mean stiffness values calculated using the equipartition theorem over this range are 26% and 34% for the 4 and 8 μm beads, respectively. Therefore, we regard the equipartition theorem as a less accurate method in calibrating optical trap stiffness as compared with the PSD and viscous drag force methods.

3.2.4 *Passive stiffness calibration based on Boltzmann statistics method*

In Fig. 5, optical trap stiffness values, estimated by the modified Boltzmann statistics calibration method using the CCD camera as position sensing means, are presented as a function of trapping laser powers in the focal plane. Estimated optical trap stiffness values for the 4 μm beads ranged from $35 \pm 6.1\ \mathrm{pN} \cdot \mu\mathrm{m}^{-1}$ at 50 mW to $198.3 \pm 60.7\ \mathrm{pN} \cdot \mu\mathrm{m}^{-1}$ at 355 mW. The stiffness values for the 8 μm beads ranged from $37.1 \pm 12.9\ \mathrm{pN} \cdot \mu\mathrm{m}^{-1}$ at 50 mW to $193.8 \pm 53.2\ \mathrm{pN} \cdot \mu\mathrm{m}^{-1}$ at 355 mW. The average standard deviations from the mean stiffness values calculated using the modified Boltzmann statistics method over this range are 29% and 33% for the 4 and 8 μm beads, respectively. The trap stiffness measurements by the equipartition theorem and the modified Boltzmann statistics calibration methods for the 4 and 8 μm beads over the trapping laser power range of 50 to 504 mW are presented in Fig. 5(a) for comparison. Both calibration methods are capable of observing the size-dependent differences in optical trap stiffness within their effective range. However, the average difference of 6% between the measured stiffness for the 4 and 8 μm beads using the equipartition theorem increases to 13.6% when using the modified Boltzmann statistics method.

The average standard deviation from the mean calculated stiffness values does not change in a meaningful way between the two methods. This suggests that the decreased dependency of the stiffness calculations on the wings of the particle's position distribution in the modified Boltzmann statistics method does not introduce significant uncertainties in the calculated results. In turn, the discrepancies between the two methods become apparent as the trapping laser powers increase, resulting in fewer data points in the far bins of the trapped particles' position histogram. The classical Boltzmann statistics approach becomes limited in performance at 355 mW, while the modified Boltzmann statistics method allows for the measurements to be extended into a higher laser power of 504 mW for the 4 μm beads, measuring a stiffness of $245.7\ \mathrm{pN} \cdot \mu\mathrm{m}^{-1}$.

While the modified Boltzmann statistics also shows some improvement over the equipartition theorem in calculating the mean stiffness value for the larger particle at 504 mW, its performance could not be reliably extended into higher powers for the 8 μm bead mainly because of the higher pixel noise in tracking the larger particles. The performance of any calibration method relying on video-based position sensing method depends on the accuracy of the subpixel particle tracking algorithm used. Figure 5(c) provides an example of how the modified Boltzmann statistics approach is limited in performance using the same bead image sets as tracked by the centroid

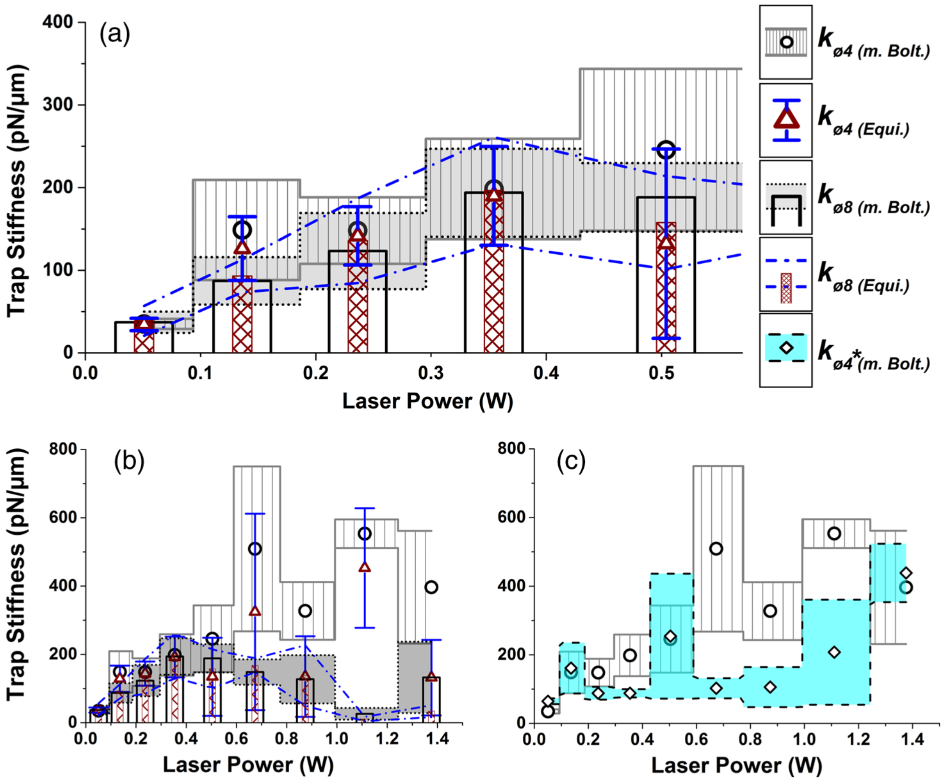

Fig. 5 Trap stiffness as a function of laser power at the specimen plane for 4 and 8 μm beads, using passive stiffness calibration methods based on the Boltzmann statistics and the equipartition theorem. The $k_{\text{Ø4 (m. Bolt.)}}$ data points (represented as circles) and $k_{\text{Ø4 (Equi.)}}$ data points (represented as triangles) correspond to the estimated stiffness values for the 4 μm beads using the modified Boltzmann statistics and the equipartition theorem, respectively. The $k_{\text{Ø8 (m. Bolt.)}}$ data points (represented as unfilled columns) and $k_{\text{Ø8 (Equi.)}}$ data points (represented as shaded columns) correspond to the estimated stiffness values for the 8 μm beads using the modified Boltzmann statistics and the equipartition theorem methods, respectively. Particles in the aforementioned data sets were tracked using the radial symmetry method. The $k_{\text{Ø4}*\text{(m. Bolt.)}}$ data points (represented as diamonds) correspond to the estimated stiffness values for the 4 μm beads using the same particles images and calibration methods as in $k_{\text{Ø4 (m. Bolt.)}}$, but with the centroid method used to track the optically trapped particles. The standard deviations from the mean measured stiffness values at each trapping laser power are shown as error bars. The error bars to the estimated stiffness values $k_{\text{Ø4 (m. Bolt.)}}$, $k_{\text{Ø4 (Equi.)}}$, and $k_{\text{Ø4}*\text{(m. Bolt.)}}$ are represented by solid horizontal lines, capped vertical lines, and dashed horizontal lines, respectively. The error bars to the estimated stiffness values $k_{\text{Ø8 (m. Bolt.)}}$ and $k_{\text{Ø8 (Equi.)}}$ are represented by dotted horizontal lines and a dash-dot spline, respectively. (a) Stiffness values $k_{\text{Ø4 (m. Bolt.)}}$, $k_{\text{Ø4 (Equi.)}}$, $k_{\text{Ø8 (m. Bolt.)}}$, and $k_{\text{Ø8 (Equi.)}}$ at lower trapping laser powers (0.05 to 0.55 W). (b) Stiffness values $k_{\text{Ø4 (m. Bolt.)}}$, $k_{\text{Ø4 (Equi.)}}$, $k_{\text{Ø8 (m. Bolt.)}}$, and $k_{\text{Ø8 (Equi.)}}$ over an extended range of trapping laser powers (0.05 to 1.5 W). Neither of the approaches produced reliable stiffness results at trapping laser powers >0.5 W. (c) Dependence of the measured trap stiffness on the particle tracking algorithm.

particle tracking algorithm, a tracking algorithm that provides less accuracy and larger pixel noise for subpixel particle tracking.[86]

The optical trap stiffness values estimated using the Boltzmann statistics method is directly related to the absolute temperature of the trapping medium [Eq. (6)]. Similar to the equipartition theorem method, in our system, the trap stiffness is underestimated by 1.4% at the trapping power of 504 mW using the Boltzmann statistics method if laser-induced temperature increase at the focus is not accounted for.

4 Discussion

We summarize the results from our stiffness calibration methods at trapping laser powers ranging from 50 mW to 1.38 W in Fig. 6. Horizontal and vertical axes are plotted on logarithmic scales to enhance the visibility at lower powers where the measured stiffness values are in close proximity. To enhance the comparison between the trapping laser power increments and estimated stiffness changes using each calibration method, the inset shows the results of the four stiffness calibration methods but with its vertical and horizontal axes, respectively, divided by the stiffness and laser power values of the smallest data points plotted ($35\ \text{pN} \cdot \mu\text{m}^{-1}$ for the modified Boltzmann statistics method using the 4 μm bead at 50 mW). The results of each stiffness calibration method are considered reliable within the trapping laser power range where a linear increase in the trap stiffness with increasing laser power is estimated. Discrepancies exist between the methods in the trap stiffness values reported at a given trapping laser power, the slope of their stiffness versus laser power, and the sensitivity of each approach in observing the size-dependent optical trap stiffness changes. While the trap stiffness estimated by all calibration methods are in good

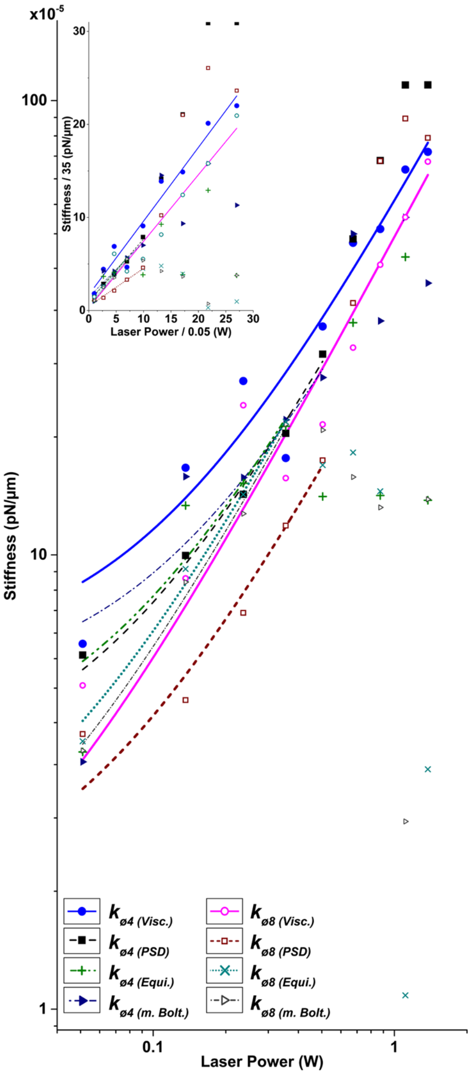

Fig. 6 Summary of the results of four stiffness calibration methods using beads with two different mean diameters (4 and 8 μm). Horizontal and vertical axes are plotted in logs to enhance the visibility at lower powers where the measured stiffness values are in close proximity. Stiffness values $k_{Ø4\,(\mathrm{Visc.})}$ and $k_{Ø8\,(\mathrm{Visc.})}$ were measured using the viscous drag force calibration and are represented as filled circles and unfilled circles, respectively. The $k_{Ø4\,(\mathrm{PSD})}$ and $k_{Ø8\,(\mathrm{PSD})}$ data sets (represented as filled squares and unfilled squares, respectively) correspond to stiffness results estimated using the power spectral density method. The results of the equipartition theorem stiffness calibration method, $k_{Ø4\,(\mathrm{Equi.})}$ and $k_{Ø8\,(\mathrm{Equi.})}$, are represented with plus and cross signs, respectively. The results of the Boltzmann statistics method, $k_{Ø4\,(\mathrm{m.\,Bolt.})}$ and $k_{Ø8\,(\mathrm{m.\,Bolt.})}$, are represented with rightward pointing filled triangles and rightward pointing unfilled triangles, respectively. The linear fits to the estimated stiffness values using the viscous drag force calibration methods, $k_{Ø4\,(\mathrm{Visc.})}$ and $k_{Ø8\,(\mathrm{Visc.})}$, are represented as thick solid lines. The linear fits to the estimated stiffness values using the power spectral density method, $k_{Ø4\,(\mathrm{PSD})}$ and $k_{Ø8\,(\mathrm{PSD})}$, are represented as a dashed line and a short-dash line, respectively. The linear fits to the estimated stiffness values using the equipartition theorem calibration method, $k_{Ø4\,(\mathrm{Equi.})}$ and $k_{Ø8\,(\mathrm{Equi.})}$, are represented by a dash-dot-dot and a dotted line, respectively. The linear fits to the estimated stiffness values using the Boltzmann statistics method, $k_{Ø4\,(\mathrm{m.\,Bolt.})}$ and $k_{Ø8\,(\mathrm{m.\,Bolt.})}$, are represented by a dash-dot and a short dash-dot, respectively. The inset shows the results of the four stiffness calibration methods but with its vertical and horizontal axes divided by the stiffness and laser power values of the smallest data points plotted (35 $\mathrm{pN} \cdot \mu\mathrm{m}^{-1}$ and 0.05 W, respectively) to enhance the comparison between the trapping laser power increments and estimated stiffness changes using each calibration method.

agreements at lower trapping laser powers, discrepancies between the methods become more apparent at higher trapping laser powers.

Extrapolation of the power-stiffness fits in Fig. 6 reveals nonzero stiffness values at zero trapping power. Optical trapping is not achieved until the optical forces experienced by the particle surpass the forces exerted on the particle by random collisions of the trapping medium. Zero stiffness as measured by the equipartition theorem indicates that the position variance of the particle approaches infinity. In Boltzmann statistics, a flat position histogram is required to assume zero stiffness. Neither of these cases is realized in practice given the limited spatial range of the position sensing devices and the limited duration of the observations. In the viscous drag force approach where the optical trap is modeled by Hooke's law, zero stiffness is realized if infinitesimally small forces result in infinitely large movements. This is not achieved since even in the absence of the trapping laser, frictional forces counter the free diffusion of the particle in the trapping medium.[90]

While these physical constraints restrict the measurement of zero stiffness at zero trapping laser power, position sensing errors are mainly responsible for the residual values measured by extrapolating the power-stiffness (or displacement-force) fits toward the origin. Minor position calibration errors and noise can lead to an overall under- (or over-) estimation of trap stiffness at each power, giving rise to residual stiffness values at zero trapping laser power. Similarly, small imperfections in the alignment of the position sensing device with the center of the trap will result in measuring residual forces at zero displacement, in both the viscous drag force and Boltzmann statistics methods. At low trapping laser powers, position sensing noise shifts the displacement-force graph in the positive direction of the displacement axis resulting in apparent negative residual forces. At higher trapping laser powers, the increased scattering force results in an axial displacement of the particle when lateral forces are applied.[91] This axial displacement is not bilateral and occurs along the coma axis,[74] resulting in a small lateral bias in measuring bead's displacements. This, in turn, shifts the force-displacement graph upward, resulting in an increased apparent residual force at zero displacement.

Laser-induced temperature increase was considered in estimating all of the results presented in Fig. 6. Not accounting for the temperature increase at higher laser powers results in underestimating the trap stiffness when using the equipartition theorem and Boltzmann statistics calibration methods, and overestimating the stiffness in PSD and viscous drag force calibration approaches. Increases in the absolute temperature of the trapping media are directly associated with increases in the stiffness value estimated by equipartition theorem and Boltzmann statistics calibration methods. However, increased temperature of the trapping media is directly associated with decreases in the stiffness values estimated by the viscous drag and PSD calibration methods because of the inverse effect of temperature with the dynamic viscosity of the trapping media and drag coefficient, β.

The sensitivity of the stiffness calibration methods to the effects of temperature increase depends on the thermal characteristics of the trapping medium and the trapping laser power range. In our case, we assumed a temperature increase of 8 K/W for our DI water trapping medium. Given the small contribution of bead properties to the laser-induced heating in optical traps,[78] the low absorption of water at 1064 nm, and the range of laser power used, this assumption remains acceptable for the purpose of our comparative study of stiffness calibration methods. Moreover, a 50% error in this assumption (8 ± 4 K/W) does not change the overall trend of the results and changes the measured stiffness by 0.1 to 1.9% using the equipartition and Boltzmann statistics methods, and 0.5 to 11% using the viscous drag force and PSD methods over the range of laser powers used in this study. Results of the PSD and viscous drag force calibration methods were more sensitive to the temperature increments compared with those of the equipartition theorem and Boltzmann statistics calibration methods. This is due to the larger temperature-induced changes in water's dynamic viscosity (20.6% decrease) compared with the absolute temperature change (3.6% increase) within the laser power range used in our study.

QPD and other nonvideo position sensing devices offer nanometer spatial resolution at kilohertz sampling frequencies, but to achieve their highest spatial resolution often requires superluminescence or laser illumination, which entails special optics and careful alignment and calibration. In return, at a lower cost compared with high-speed cameras, the QPD can be used to characterize optical traps in studies involving high trapping laser powers. We used the QPD in an imaging configuration that offers less spatial resolution than the back focal plane interferometry configuration. The limited spatial and temporal resolution of position sensing is the limiting factor in the efficiency of calibration methods at higher trapping laser powers. Any enhancement of the position sensing accuracy and precision will, in turn, enhance the efficiency of the stiffness calibration methods.

Cameras with low pixel noise can offer nanometer spatial resolution for simultaneous tracking of multiple objects in conjunction with subpixel particle tracking algorithms. At a cost comparable with the nonvideo position sensing means, cameras with native acquisition rates of several hundred frames per second can be used at a few kilohertz frame rates through binning. This frame rate is sufficient to perform frequency analysis of the thermal fluctuations of large optically trapped particles.[92] However, high-speed CMOS sensors and line scan cameras are still required to achieve a comparable temporal resolution offered by the nonvideo position sensing means (tens of kilohertz) needed for particles in the Rayleigh regime. Currently, these ultrafast video position sensing schemes are often costly and limited in performance compared with their nonvideo counterparts. However, common video acquisition rates of >100 Hz can be used to determine the stiffness of an optical trap in most biophysical applications where the trapping laser power is limited to prevent optical damage to the samples.

Stiffness calibration methods using the equipartition theorem and Boltzmann statistics measure the thermal vibrations of a trapped particle to estimate the trap stiffness. In the equipartition theorem method, position variance is directly used to estimate the stiffness, whereas Boltzmann statistics calibration method reconstructs a normalized probability function based on the distribution of trapped particle's positions in the optical trap to measure the stiffness. Thus, Boltzmann statistics method is less sensitive to the white noise in the measurement instrumentation, which when using the equipartition theorem, can cause underestimation of the trap stiffness by adding to the apparent variance of the particle position. The statistical nature of the Boltzmann method enhances the spatial resolution of the system in reconstructing the probability function of the trapped particle's position.

The equipartition theorem method requires the least amount of postprocessing for calibrating the stiffness of an optical trap compared with the other methods in this study. Because the position variance is a biased (always positive) estimator, the equipartition theorem is more sensitive to the position detection noise, detector's spatial and temporal resolution, and detector's position calibration errors compared with the other calibration methods. This bias decreases the usefulness of the equipartition theorem calibration method when nonvideo position sensing means with intrinsic high-frequency noise are used. This issue can be addressed by low-pass filtering the position signal, but care must be taken to account for the effects of filtering parameters on the information content of the signal.[27]

Compared with the equipartition theorem, the Boltzmann statistics method suffers less position detector related errors in estimating optical trap stiffness over the range of trapping laser powers. The Boltzmann statistics method can also be used to study the optical trap's potential energy shape. On the other hand, the probability distribution function in the Boltzmann statistics method is a continuous function fitted to discrete position data points. Therefore, the estimated optical trap stiffness values are sensitive to fitting parameters, such as the bin size and the fitting function. We used a modified Boltzmann statistics approach, which improved the efficiency of the method at higher trapping laser powers and enhanced its sensitivity to particle diameter dependent variations in optical trap stiffness.

Neither the Boltzmann statistics nor the equipartition theorem calibration methods require calculating the drag coefficient of the trapped particles, making them suitable for studies that involve trapping cell and particles of arbitrary shapes. At a given position sensing temporal and spatial resolution, both equipartition theorem and Boltzmann statistics methods are more suitable for studying weaker optical traps with smaller optically trapped objects. Compared with the PSD and viscous drag force approaches, the equipartition theorem and Boltzmann statistics stiffness calibration methods have a limited laser power range in which they can reliably be used to calibrate the optical trap stiffness and offer smaller confidence in the measured stiffness.

At higher trapping powers, the viscous drag force and PSD calibration methods are more reliable for calibrating the trap stiffness. Compared with the results from other calibration methods, the PSD method has the highest sensitivity to the particle size dependent changes in trap stiffness. Studying the PSD of an optically trapped particle can also provide valuable information about the electrical and mechanical noise present in the trapping system.[93] Moreover, this method can be used for directly calibrating the position sensing device when a motorized or PZT stage is not available,[94] as well as extracting the drag coefficient for trapped particles of arbitrary shapes.[57]

Discrete numerical methods used in the PSD estimation affect the Lorentzian shape of the PSD. The low-pass effect of the position sensing diodes as well as a number of other physical and theoretical approximations[41] can affect the accuracy of the apparent roll-off frequency. Free software packages are developed and are available online that can be used to compensate for these factors[42,95,96] when calibrating an optical trap stiffness using the PSD method. Although the position sensing device needs not to be displacement-calibrated when using the PSD calibration method, a high spatial resolution is crucial in order to observe small thermal vibrations of the particle inside stronger optical traps, ultimately affecting the efficacy of the PSD calibration method at higher trapping laser powers.

Position detection spatial resolution is limited to the nanometer range even with the most sensitive laser based position sensing schemes, such as back focal plane interferometry. At higher trapping laser powers where the thermal movements of the optically trapped particle approach the spatial resolution limits of the position sensing system, active stiffness calibration methods can produce more reliable calibration results. Controlled viscous forces (and subsequently particle displacements from the center of the trap) can be induced to overcome the low positional SNR in stronger optical traps.

Calibrating optical tweezers' stiffness using known viscous drag forces requires the most postprocessing effort. Accuracy of the results depends on the exact knowledge of particle size and drag coefficient, temperature and viscous properties of the medium, and having a displacement-calibrated position detection system. Motorized or PZT stages (or microfluidic trapping chambers with precise control over the flow rate) are required with active stiffness calibration methods for applying known displacements or viscous forces on optically trapped particles. In return, calibrating the optical trap against known viscous drag forces provides the most accurate and relevant stiffness results for studies involving large displacements of the trapped particle from the center of the optical trap.

Acknowledgments

This work was supported in part by a grant from the National Institutes of Health (2R01-DC02775) and National Science Foundation (BES-0522862). Additional support was provided by Bourns College of Engineering and the Center for Bioengineering Research at the University of California, Riverside.

References

1. A. Ashkin, "Acceleration and trapping of particles by radiation pressure," *Phys. Rev. Lett.* **24**(4), 156 (1970).
2. C. G. Baumann et al., "Stretching of single collapsed DNA molecules," *Biophys. J.* **78**(4), 1965–1978 (2000).
3. S. M. Block, D. F. Blair, and H. C. Berg, "Compliance of bacterial flagella measured with optical tweezers," *Nature* **338**(6215), 514–518 (1989).
4. J. Sleep et al., "Elasticity of the red cell membrane and its relation to hemolytic disorders: an optical tweezers study," *Biophys. J.* **77**(6), 3085–3095 (1999).
5. S. Hénon et al., "A new determination of the shear modulus of the human erythrocyte membrane using optical tweezers," *Biophys. J.* **76**(2), 1145–1151 (1999).
6. K. Svoboda and S. M. Block, "Biological applications of optical forces," *Annu. Rev. Biophys. Biomol. Struct.* **23**(1), 247–285 (1994).
7. M. Dao, C. T. Lim, and S. Suresh, "Mechanics of the human red blood cell deformed by optical tweezers," *J. Mech. Phys. Solids* **51**(11–12), 2259–2280 (2003).
8. C. T. Lim et al., "Large deformation of living cells using laser traps," *Acta Mater.* **52**(7), 1837–1845 (2004).
9. J. Dai and M. P. Sheetz, "Mechanical properties of neuronal growth cone membranes studied by tether formation with laser optical tweezers," *Biophys. J.* **68**(3), 988–996 (1995).
10. D. Choquet, D. P. Felsenfeld, and M. P. Sheetz, "Extracellular matrix rigidity causes strengthening of integrin-cytoskeleton linkages," *Cell* **88**(1), 39–48 (1997).
11. M. M. Brandão et al., "Optical tweezers for measuring red blood cell elasticity: application to the study of drug response in sickle cell disease," *Eur. J. Haematol.* **70**(4), 207–211 (2003).
12. P. J. Bronkhorst et al., "A new method to study shape recovery of red blood cells using multiple optical trapping," *Biophys. J.* **69**(5), 1666–1673 (1995).
13. R. R. Huruta et al., "Mechanical properties of stored red blood cells using optical tweezers," *Blood* **92**(8), 2975–2977 (1998).
14. G.-B. Liao et al., "One-dimensional jumping optical tweezers for optical stretching of bi-concave human red blood cells," *Opt. Express* **16**(3), 1996–2004 (2008).
15. K. Svoboda et al., "Conformation and elasticity of the isolated red blood cell membrane skeleton," *Biophys. J.* **63**(3), 784–793 (1992).
16. Y. Li et al., "Mechanical property analysis of stored red blood cell using optical tweezers," *Colloids Surf. B* **70**(2), 169–173 (2009).
17. A. Ashkin, "History of optical trapping and manipulation of small-neutral particle, atoms, and molecules," *IEEE J. Sel. Topics Quantum Electron.* **6**(6), 841–856 (2000).
18. A. Ashkin, "Optical trapping and manipulation of neutral particles using lasers," *Proc. Natl. Acad. Sci. U.S.A.* **94**(10), 4853–4860 (1997).
19. T. L. Gustavson et al., "Transport of Bose-Einstein condensates with optical tweezers," *Phys. Rev. Lett.* **88**(2), 020401 (2001).
20. M. D. Barrett, J. A. Sauer, and M. S. Chapman, "All-optical formation of an atomic Bose-Einstein condensate," *Phys. Rev. Lett.* **87**(1), 010404 (2001).
21. L. P. Ghislain and W. W. Webb, "Scanning-force microscope based on an optical trap," *Opt. Lett.* **18**(19), 1678–1680 (1993).
22. Y. Arai et al., "Tying a molecular knot with optical tweezers," *Nature* **399**(6735), 446–448 (1999).
23. W. B. Richard and J. P. Miles, "Optical trapping and binding," *Rep. Prog. Phys.* **76**(2), 026401 (2013).
24. S. Khan and M. P. Sheetz, "Force effects on biochemical kinetics," *Annu. Rev. Biochem.* **66**, 785–805 (1997).
25. T. Nishizaka et al., "Unbinding force of a single motor molecule of muscle measured using optical tweezers," *Nature* **377**(6546), 251–254 (1995).
26. M. D. Wang et al., "Stretching DNA with optical tweezers," *Biophys. J.* **72**(3), 1335–1346 (1997).
27. K. C. Neuman and A. Nagy, "Single-molecule force spectroscopy: optical tweezers, magnetic tweezers and atomic force microscopy," *Nat. Methods* **5**(6), 491–505 (2008).
28. Z. Li et al., "Membrane tether formation from outer hair cells with optical tweezers," *Biophys. J.* **82**(3), 1386–1395 (2002).
29. S. A. Ermilov et al., "Studies of plasma membrane mechanics and plasma membrane-cytoskeleton interactions using optical tweezers and fluorescence imaging," *J. Biomech.* **40**(2), 476–480 (2007).
30. N. Khatibzadeh et al., "Effects of cholesterol on nano-mechanical properties of the living cell plasma membrane," *Soft Matter* **8**(32), 8350–8360 (2012).
31. N. Khatibzadeh et al., "Effects of plasma membrane cholesterol level and cytoskeleton f-actin on cell protrusion mechanics," *PLoS ONE* **8**(2), e57147 (2013).
32. A. Ashkin and J. M. Dziedzic, "Internal cell manipulation using infrared laser traps," *Proc. Natl. Acad. Sci. U.S.A.* **86**(20), 7914–7918 (1989).
33. A. G. Hendricks, E. L. F. Holzbaur, and Y. E. Goldman, "Forces in intracellular transport: calibrated optical trap recordings in living cells," *Biophys. J.* **102**(3), 38a (2012).
34. R. W. Steubing et al., "Laser induced cell fusion in combination with optical tweezers: the laser cell fusion trap," *Cytometry* **12**(6), 505–510 (1991).
35. J. Mas et al., "Quantitative determination of optical trapping strength and viscoelastic moduli inside living cells," *Phys. Biol.* **10**(4), 046006 (2013).
36. H. Felgner, O. Müller, and M. Schliwa, "Calibration of light forces in optical tweezers," *Appl. Opt.* **34**(6), 977–982 (1995).
37. F. Gittes and C. F. Schmidt, "Interference model for back-focal-plane displacement detection in optical tweezers," *Opt. Lett.* **23**(1), 7–9 (1998).
38. W. Singer et al., "Three-dimensional force calibration of optical tweezers," *J. Mod. Opt.* **47**(14–15), 2921–2931 (2000).
39. W. Grange et al., "Optical tweezers system measuring the change in light momentum flux," *Rev. Sci. Instrum.* **73**(6), 2308–2316 (2002).
40. S. Ermilov and B. Anvari, "Dynamic measurements of transverse optical trapping force in biological applications," *Ann. Biomed. Eng.* **32**(7), 1016–1026 (2004).
41. S. K. Berg and H. Flyvbjerg, "Power spectrum analysis for optical tweezers," *Rev. Sci. Instrum.* **75**(3), 594–612 (2004).
42. I. M. Tolic-Nørrelykke, K. Berg-Sørensen, and H. Flyvbjerg, "Matlab program for precision calibration of optical tweezers," *Comput. Phys. Commun.* **159**(3), 225–240 (2004).

43. B.-J. Chang, L. Hsu, and S. Chi, "Rapid and simple automatic trapping-force calibration system for optical tweezers," *Opt. Eng.* **44**(11), 113603–113605 (2005).
44. N. B. Viana et al., "Absolute calibration of optical tweezers," *Appl. Phys. Lett.* **88**(13), 131110–131113 (2006).
45. W. P. Wong and K. Halvorsen, "The effect of integration time on fluctuation measurements: calibrating an optical trap in the presence of motion blur," *Opt. Express* **14**(25), 12517–12531 (2006).
46. M. Klein et al., "Dual-trap technique for reduction of low-frequency noise in force measuring optical tweezers," *Appl. Opt.* **46**(3), 405–412 (2007).
47. W. M. Lee et al., "Construction and calibration of an optical trap on a fluorescence optical microscope," *Nat. Protoc.* **2**(12), 3226–3238 (2007).
48. J. P. Sharpe, C. Iniguez-Palomares, and R. Jimenez-Flores, "Optical tweezers force calibration using a fast-shuttering camera," in *Imaging, Manipulation, and Analysis of Biomolecules, Cells, and Tissues V*, Daniel L. Farkas, Robert C. Leif, and Dan V. Nicolau, Eds., pp. 644114–644118, SPIE, San Jose, CA (2007).
49. A. Van der Horst and N. R. Forde, "Calibration of dynamic holographic optical tweezers for force measurements on biomaterials," *Opt. Express* **16**(25), 20987–21003 (2008).
50. A. Farré and M. Montes-Usategui, "A force detection technique for single-beam optical traps based on direct measurement of light momentum changes," *Opt. Express* **18**(11), 11955–11968 (2010).
51. M. Fischer et al., "Active-passive calibration of optical tweezers in viscoelastic media," *Rev. Sci. Instrum.* **81**(1), 015103–015110 (2010).
52. N. Osterman, "Tweezpal—optical tweezers analysis and calibration software," *Comput. Phys. Commun.* **181**(11), 1911–1916 (2010).
53. W. H. Wright, G. J. Sonek, and M. W. Berns, "Parametric study of the forces on microspheres held by optical tweezers," *Appl. Opt.* **33**(9), 1735–1748 (1994).
54. G. Lenormand et al., "Direct measurement of the area expansion and shear moduli of the human red blood cell membrane skeleton," *Biophys. J.* **81**(1), 43–56 (2001).
55. R. M. Simmons et al., "Quantitative measurements of force and displacement using an optical trap," *Biophys. J.* **70**(4), 1813–1822 (1996).
56. A. Le Gall et al., "Simultaneous calibration of optical tweezers spring constant and position detector response," *Opt. Express* **18**(25), 26469–26474 (2010).
57. S. F. Tolić-Nørrelykke et al., "Calibration of optical tweezers with positional detection in the back focal plane," *Rev. Sci. Instrum.* **77**(10), 103101 (2006).
58. E. L. Florin et al., "Photonic force microscope calibration by thermal noise analysis," *Appl. Phys. A* **66**(1), S75–S78 (1998).
59. M.-T. Wei and A. Chiou, "Three-dimensional tracking of Brownian motion of a particle trapped in optical tweezers with a pair of orthogonal tracking beams and the determination of the associated optical force constants," *Opt. Express* **13**(15), 5798–5806 (2005).
60. M.-T. Wei et al., "Three-dimensional optical force field on a Chinese hamster ovary cell in a fiber-optical dual-beam trap," *Opt. Express* **14**(7), 3056–3064 (2006).
61. M. Ribezzi-Crivellari, J. M. Huguet, and F. Ritort, "Counter-propagating dual-trap optical tweezers based on linear momentum conservation," *Rev. Sci. Instrum.* **84**(4), 043104 (2013).
62. S. B. Smith, Y. Cui, and C. Bustamante, "Optical-trap force transducer that operates by direct measurement of light momentum," *Methods Enzymol.* **361**, 134–162 (2003).
63. A. Farré, F. Marsà, and M. Montes-Usategui, "Optimized back-focal-plane interferometry directly measures forces of optically trapped particles," *Opt. Express* **20**(11), 12270–12291 (2012).
64. J. P. Mills et al., "Nonlinear elastic and viscoelastic deformation of the human red blood cell with optical tweezers," *Mech. Chem. Biosyst.* **1**(3), 169–180 (2004).
65. F. Qian et al., "Combining optical tweezers and patch clamp for studies of cell membrane electromechanics," *Rev. Sci. Instrum.* **75**(9), 2937–2942 (2004).
66. O. M. Marago et al., "Optical trapping and manipulation of nanostructures," *Nat. Nano* **8**(11), 807–819 (2013).
67. P. M. Hansen et al., "Expanding the optical trapping range of gold nanoparticles," *Nano Lett.* **5**(10), 1937–1942 (2005).
68. A. Ashkin, "Forces of a single-beam gradient laser trap on a dielectric sphere in the ray optics regime," *Biophys. J.* **61**(2), 569–582 (1992).
69. W. H. Wright, G. J. Sonek, and M. W. Berns, "Radiation trapping forces on microspheres with optical tweezers," *Appl. Phys. Lett.* **63**(6), 715–717 (1993).
70. A. Rohrbach, "Stiffness of optical traps: quantitative agreement between experiment and electromagnetic theory," *Phys. Rev. Lett.* **95**(16), 168102 (2005).
71. P. A. M. Neto and H. M. Nussenzveig, "Theory of optical tweezers," *Europhys. Lett.* **50**(5), 702 (2000).
72. A. Mazolli, P. A. M. Neto, and H. M. Nussenzveig, "Theory of trapping forces in optical tweezers," *Proc. R. Soc. A* **459**(2040), 3021–3041 (2003).
73. N. B. Viana et al., "Towards absolute calibration of optical tweezers," *Phys. Rev. E* **75**(2), 021914 (2007).
74. R. S. Dutra et al., "Absolute calibration of forces in optical tweezers," *Phys. Rev. A* **90**(1), 013825 (2014).
75. K. Svoboda and S. M. Block, "Optical trapping of metallic Rayleigh particles," *Opt. Lett.* **19**(13), 930–932 (1994).
76. M. Haghshenas-Jaryani et al., "Dynamics of microscopic objects in optical tweezers: experimental determination of underdamped regime and numerical simulation using multiscale analysis," *Nonlinear Dyn.* **76**(2), 1013–1030 (2014).
77. K. C. Neuman and S. M. Block, "Optical trapping," *Rev. Sci. Instrum.* **75**(9), 2787–2809 (2004).
78. E. J. G. Peterman, F. Gittes, and C. F. Schmidt, "Laser-induced heating in optical traps," *Biophys. J.* **84**(2), 1308–1316 (2003).
79. K. C. Neuman et al., "Characterization of photodamage to escherichia coli in optical traps," *Biophys. J.* **77**(5), 2856–2863 (1999).
80. H. Misawa et al., "Three–dimensional optical trapping and laser ablation of a single polymer latex particle in water," *J. Appl. Phys.* **70**(7), 3829–3836 (1991).
81. K. Svoboda and S. M. Block, "Force and velocity measured for single kinesin molecules," *Cell* **77**(5), 773–784 (1994).
82. K. C. Vermeulen et al., "Optical trap stiffness in the presence and absence of spherical aberrations," *Appl. Opt.* **45**(8), 1812–1819 (2006).
83. A. Pralle et al., "Three-dimensional high-resolution particle tracking for optical tweezers by forward scattered light," *Microsc. Res. Tech.* **44**(5), 378–386 (1999).
84. M. Mahamdeh and E. Schaffer, "Optical tweezers with millikelvin precision of temperature-controlled objectives and base-pair resolution," *Opt. Express* **17**(19), 17190–17199 (2009).
85. Q. Tian and M. N. Huhns, "Algorithms for subpixel registration," *CVGIP* **35**(2), 220–233 (1986).
86. R. Parthasarathy, "Rapid, accurate particle tracking by calculation of radial symmetry centers," *Nat. Methods* **9**(7), 724–726 (2012).
87. J. C. Crocker and D. G. Grier, "Methods of digital video microscopy for colloidal studies," *J. Colloid Interface Sci.* **179**(1), 298–310 (1996).
88. O. Otto et al., "Optical tweezers with 2.5 khz bandwidth video detection for single-colloid electrophoresis," *Rev. Sci. Instrum.* **79**(2), 023710 (2008).
89. A. van der Horst and N. R. Forde, "Power spectral analysis for optical trap stiffness calibration from high-speed camera position detection with limited bandwidth," *Opt. Express* **18**(8), 7670–7677 (2010).
90. R. Kubo, "The fluctuation-dissipation theorem," *Rep. Prog. Phys.* **29**(1), 255 (1966).
91. F. Merenda et al., "Escape trajectories of single-beam optically trapped micro-particles in a transverse fluid flow," *Opt. Express* **14**(4), 1685–1699 (2006).
92. S. Keen et al., "Comparison of a high-speed camera and a quadrant detector for measuring displacements in optical tweezers," *J. Opt. A-Pure Appl. Opt.* **9**(8), S264 (2007).
93. F. Czerwinski, A. C. Richardson, and L. B. Oddershede, "Quantifying noise in optical tweezers by allan variance," *Opt. Express* **17**(15), 13255–13269 (2009).
94. M. W. Allersma et al., "Two-dimensional tracking of ncd motility by back focal plane interferometry," *Biophys. J.* **74**(2), 1074–1085 (1998).
95. P. M. Hansen et al., "Tweezercalib 2.1: faster version of Matlab package for precise calibration of optical tweezers," *Comput. Phys. Commun.* **175**(8), 572–573 (2006).
96. P. M. Hansen et al., "Tweezercalib 2.0: faster version of Matlab package for precise calibration of optical tweezers," *Comput. Phys. Commun.* **174**(6), 518–520 (2006).

Biographies of the authors are not available.